Charge Transfer in a Multi-Implant Pinned-Buried Photodetector

R. K. Jarwal, Durga Misra, *Senior Member, IEEE*, and John L. Lowrance, *Life Senior Member, IEEE*

***Abstract*—This work presents a charge transfer model for a multi-implant (graded) pinned-buried photodetector for high frame rate imaging applications. The model takes into account the initial charge of each implanted region which is divided into a large number of small areas and the maximum effective transit length of the far and near electrons by taking into account the fringing field effect due to graded implants under uniform illumination condition. The model predicts 1.5 μs for a single-implant and 500 ns for a three-implant photodetector for collection of 90% of the initial charge. The computed values agree well with the experimental results for a three-implant 70 μm $\times$ 45 μm photodetector measured at a rate of 10^6 frames/s with uniformly illuminated by 100 ns LED pulses.**

***Index Terms*—Charge transfer, high frame rate image sensors, photodetector, transit time.**

I. Introduction

IMAGE acquisition at very high frame rate is required for studying rapid mechanical motion and transient phenomena such as optical wavefront measurements, explosion study and hypersonic gas turbulence imaging. The required time resolution for such applications is between 0.1 μs to 1 μs. To meet this requirement burst image sensors with very high frame rate were developed [1]–[8]. These image sensors are designed to capture images at frame rate 10^6 frames/s or higher by continuously storing the last frames at the pixel location. In general, an $n \times n$ element image sensor is designed in the form of four quadrants each with $n/2 \times n/2$ pixels, where n is the number of pixels. Each pixel consists of a photodetector and series-parallel combination of buried-channel charge-coupled device (BCCD) registers for continuously storing the last image frames. The imager with a large photodetector is required to obtain a complete charge readout in much less than 1.0 μs. A multi-implant (graded) pinned-buried photodetector is used to reduce the effective travel time or the readout time. To achieve a high-speed detection, with essentially zero frame-to-frame lag, graded potential steps are created in the photodetector by variation of doping concentration of implants. To describe the charge transfer in the photodetector a thermal diffusion model was developed [9]. This model does not take into account the area or initial charge of individual implant and the effective transit length for near and far electrons.

Manuscript received March 27, 2000; revised November 5, 2000. This work was supported by the New Jersey Center for Optoelectronics. The review of this paper was arranged by Editor J. Hynecek.

R. K. Jarwal and D. Misra are with the Department of Electrical and Computer Engineering, New Jersey Institute of Technology, University Heights, Newark, NJ 07102-1982 USA (e-mail: dmisra@adm.njit.edu).

J. L. Lowrance is with the Princeton Scientific Instruments Inc., Monmouth Junction, NJ 08852 USA.

Publisher Item Identifier S 0018-9383(01)02343-7.

The present work studies the charge transfer characteristics of photodetector by taking into account the area or initial charge of individual implant and the effective transit length associated with near and far electrons. In this paper, the theoretical analysis is described in Section II. This section starts with a description of the effect of thermal diffusion and fringing field in a multi-implant photodetector. This is followed by the derivation of the charge transfer model where electron transfer from the individual implanted regions is considered. In Section III the results obtained by this model are compared with that of a single-implant photodetector and with the experimental results. The conclusions drawn from this work were embodied in Section IV.

II. Theoretical Analysis

To describe the photodetector charge readout time with multi-implants, a thermal diffusion model [9] was developed by taking into account free charge transfer theory in charge-coupled devices [10]. According to this model the photodetector with M n-type detector implants is made up of M constant potential regions each with an effective L_{eff} separated by a step potential of about 0.5 V. The effective photodetector charge readout time is estimated as the thermal diffusion time for the longest constant potential region plus an effective charge transfer between these regions. The cross-sectional view of a three-n type implant pinned-buried photodetector is shown in Fig. 1(a). The implant concentration N_1 is BCCD implant plus the first photodetector implant, N_2 is N_1 plus second photodetector implant, and N_3 is N_2 plus the third photodetector implant. These three implants result in a graded potential profile along the photodetector as shown in Fig. 1(b). The potential profile divides the photodetector into three sections where section 2 acts as a charge sink for section 1, and section 3 acts as a charge sink for section 2. Finally, the potential well under the charge-collecting gate acts as a sink for the charge collected by the photodetector. The image acquisition cycle is the most important cycle of the imager. During this cycle the charge signal, which is detected by the photodetector, is transferred in series into the registers for detection of successive frames [9].

Thermal diffusion and fringing field drift govern the electron motion in a photodetector. The effect of thermal diffusion is studied by introducing the current density relation into continuity equation, and solving the partial differential equation. The solution is given by [10]

$$Q(t) = \frac{8}{\pi^2} Q(0) \exp\left[-\frac{\pi^2 D_n t}{4L^2}\right]$$
$$Q(t) = \frac{8}{\pi^2} Q(0) e^{-t/\tau} \quad (1)$$

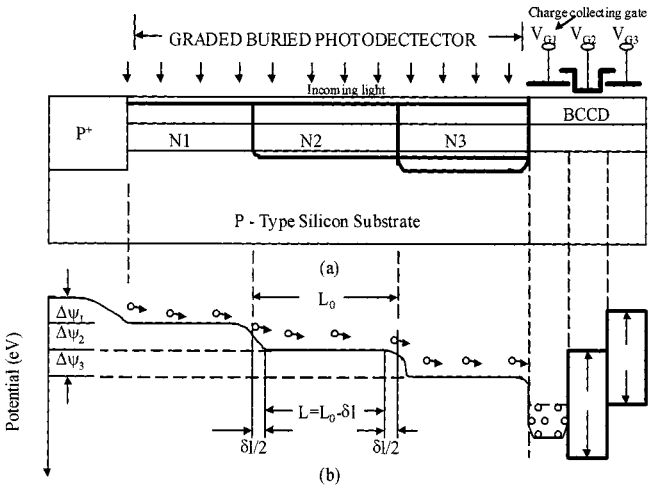

Fig. 1. Cross-sectional view of the three N-type photodetector implant (a) graded potential profile and operation (b) showing the effect of fringing fields in electron transport.

where

$Q(t)$	charge at time t;
$Q(0)$	initial charge;
D_n	diffusion coefficient;
τ	diffusion time constant;
L	transit length

shown in Fig. 1(b) is different from the lifetime in the material. The diffusion coefficient D_n is related to the electron mobility μ_n [11] by

$$D_n = \frac{\mu_n(n)kT}{e}\left[1 + 0.35335\left(\frac{n}{N_c}\right) - 9.9\times 10^{-3}\left(\frac{n}{N_c}\right)^2 + \cdots\right] \quad (2)$$

where

k	Boltzmann constant
T	temperature in degree Kelvin
e	electronic charge and
N_c	effective density of states in the conduction band.

It can be seen from (1) that charge decreases exponentially with time from its initial value. The time constant of diffusion mechanism is inversely proportional to D_n and directly proportional to the square of the transit length. For a high-speed photodetector L should be small and D_n should be large. A multi-implant photodiode, therefore, reduces the charge readout time.

The layout of a three n-type-implant pinned-buried photodetector ($70\ \mu\text{m} \times 45\ \mu\text{m}$) is shown Fig. 2. The total area of the photodiode is A and A_1, A_2 and A_3 are the areas of implant regions. The charge transfer in a photodetector takes place from the entire area. To include charge transfer from different portions of the detector it is more accurate and reasonable to divide the entire photodetector area into small areas. It is quite possible to divide the photodetector into various sizes and shapes such as circular areas or triangular areas, in that case there could be some unaccounted for or overlapping areas. As a result, the charge transfer estimation could be inaccurate. For simplicity

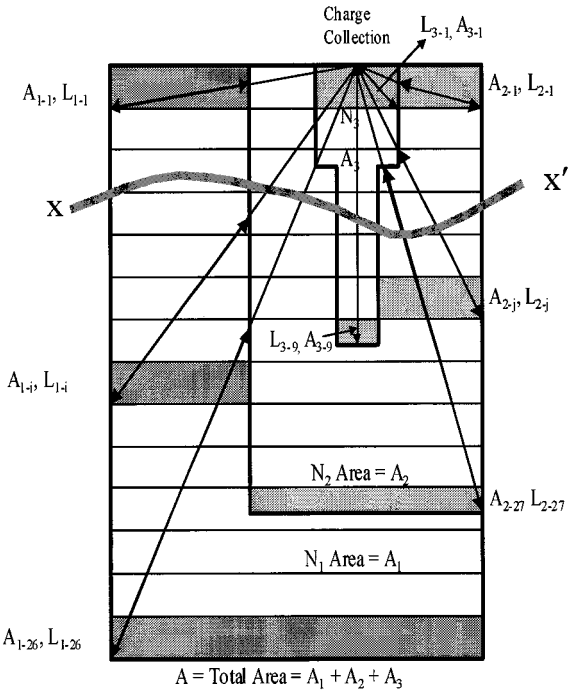

Fig. 2. Layout of a three n-type implant pinned-buried photodetector showing various small sections with associated transit lengths for electrons. Individual small sections are enlarged for clarity where x-x' indicates a break in the distribution of these small sections.

we have divided the photodetector only into small rectangular areas. The implant area A_1 is divided into $p = 26$ number of small sections with an area of A_{1-i} each. Similarly, implant area A_2 and A_3 are divided into $q = 27$ and $r = 9$ number of small sections with an area of A_{2-j} and A_{3-k} for each small sections, respectively. The ideal number of small sections could be infinite but as per the layout of the experimental photodetector the number of small areas selected here are adequate enough for this study. Increasing the number of small areas in each section beyond this does not add to significant improvements to accuracy. The total charge in the photodetector at any time t can be obtained by the superposition of charges in all small sections at time t. Mathematically it can be expressed similar to (1) as

$$Q(t) = \frac{8}{\pi^2}\frac{Q(0)}{A}\left[\sum_{i=1}^{p} A_{1-i}\exp\left[-\frac{\pi^2 D_{1n}t}{4L_{1-i}^2}\right] + \sum_{j=1}^{q} A_{2-j}\exp\left[-\frac{\pi^2 D_{2n}t}{4L_{2-j}^2}\right] + \sum_{k=1}^{r} A_{3-k}\exp\left[-\frac{\pi^2 D_{3n}t}{4L_{3-k}^2}\right]\right] \quad (3)$$

where

A_{1-i}	ith area of implant region A_1;
A_{2-j}	jth area of implant region A_2;
A_{3-k}	kth area of implant region A_3,
D_{1n}	diffusion coefficient of implant region A_1;
D_{2n}	diffusion coefficient of implant region A_2;
D_{3n}	diffusion coefficient of implant region A_3;

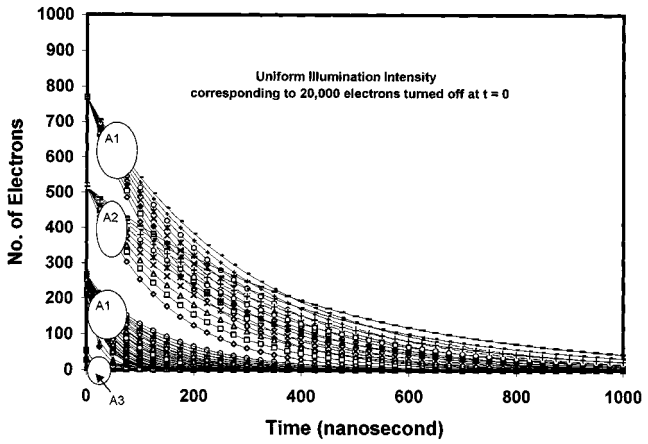

Fig. 3. Electron transfer characteristics of all small areas as a function of time for different implanted region for uniform illumination corresponding to 20 000 electrons when the illumination is turned off at $t = 0$.

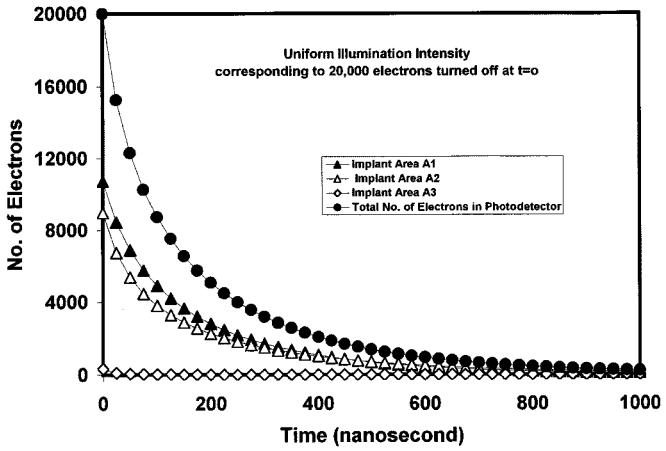

Fig. 4. Separate electron transfer characteristics of all three implanted regions and of the photodetector as a function of time for uniform illumination corresponding to 20 000 electrons when the illumination is turned off at $t = 0$.

L_{1-i} effective maximum transit length of electrons in ith area of implant region A_1;

L_{2-j} effective maximum transit length of electrons in jth area of implant region A_2,

L_{3k} effective maximum transit length of electrons in kth area of implant region A_3.

It is to be noted that one small section could be sink for some other small section. The resulting equation would be more complicated than (3). For simplicity we have kept that derivation step out of the scope of this model.

III. Results and Discussions

The experimental set-up developed by Princeton Scientific Instruments [9] for the operation of photodetector has a test pattern uniformly illuminated by 100 ns LED pulses. The switching operation of LED at any frame rate is controlled by a computer. The optical pattern is detected by the photodetector at frame rate up to 10^6 frames/s. The output signal of the photodetector is readout by dual-slope correlated-double sampling to eliminate reset noise. After analog to digital conversion, the signal is read by computer and stored. For the photodetector shown in Fig. 2, the experimental values of the doping concentrations are $N_1 \approx 1.4 \times 10^{17}\ \mathrm{cm}^{-3}$, $N_2 \approx 2.6 \times 10^{17}\ \mathrm{cm}^{-3}$ and $N_3 \approx 3.6 \times 10^{17}\ \mathrm{cm}^{-3}$ which are used in our model for electron transit time estimation. The corresponding electron mobilities for these concentrations are $\mu_{1n} \approx 700\ \mathrm{cm}^2/\mathrm{V}\cdot\mathrm{sec}$, $\mu_{2n} \approx 600\ \mathrm{cm}^2/\mathrm{V}\cdot\mathrm{sec}$, $\mu_{3n} \approx 500\ \mathrm{cm}^2/\mathrm{V}\cdot\mathrm{sec}$. These mobilities give three different diffusion coefficients $D_{1n} \approx 18.145\ \mathrm{cm}^2/\mathrm{sec}$, $D_{2n} \approx 15.576\ \mathrm{cm}^2/\mathrm{s}$, and $D_{3n} \approx 12.994\ \mathrm{cm}^2/\mathrm{s}$ for three implant regions respectively. The effective maximum transit length L of each section was computed by subtracting the length δl due to fringing fields from the physical length L_0 of the implanted region as shown in Fig. 1(b). We have neglected the transit time of electrons for δl as the electron pass over a potential step.

Fig. 3 shows the number of electrons present in each small section as a function of time after the uniform illumination intensity corresponding to 20 000 electrons incident on the photodetector is turned off at $t = 0$. It can be seen that the number of electrons transferred from a small section to the collecting gate at time t depends on its initial number of electrons and maximum effective transit length or location from the collecting gate. The electrons are transferred from nearer sections to the collecting gate in smaller time, whereas the electrons are transferred from periphery of the photodetector in longer time. On the average, the electron transfer mechanism from implant region A_1 is slowest and fastest from implant region A_3

The total number of electrons in the photodetector is obtained by the superposition of the contribution of number of electrons from each small section. Fig. 4 shows the number of electrons present in three implanted regions and the photodetector as a function of time after the uniform illumination intensity corresponding to 20 000 electrons is turned off at $t = 0$. It can be seen that electron transfer from each implant region depends on the initial number of electrons and the maximum transit length. The readout time for 90% electron transfer from each implant region is different. For the multi-implant photodetector, for 90% of electrons transfer the readout time is about 500 ns.

Present model was used to compute the charge transfer for single n-type implant photodetector ($70\ \mu\mathrm{m} \times 45\ \mu\mathrm{m}$) where N_1 was $1.4 \times 10^{17}\ \mathrm{cm}^{-3}$. The corresponding electron mobility and diffusion coefficient are $700\ \mathrm{cm}^2/\mathrm{V}\cdot\mathrm{s}$ and $18.145\ \mathrm{cm}^2/\mathrm{s}$ respectively. Fig. 5 shows the comparison of electron transfer characteristics for single n-type implant and three n-type implant photodetectors after the uniform illumination intensity corresponding to 20 000 electrons is turned off at $t = 0$. It can be seen that the charge readout time for three n-type photodetector is much smaller than one n-type implant photodetector. For 90% electron transfer the readout time for three-implant detector is about 500 ns and for single implant detector readout time is well above 1 μs.

Charge readout comparison between the experimental results measured at a frame rate of 10^6 frames/s with uniformly illuminated by 100 ns LED pulses and the results obtained by

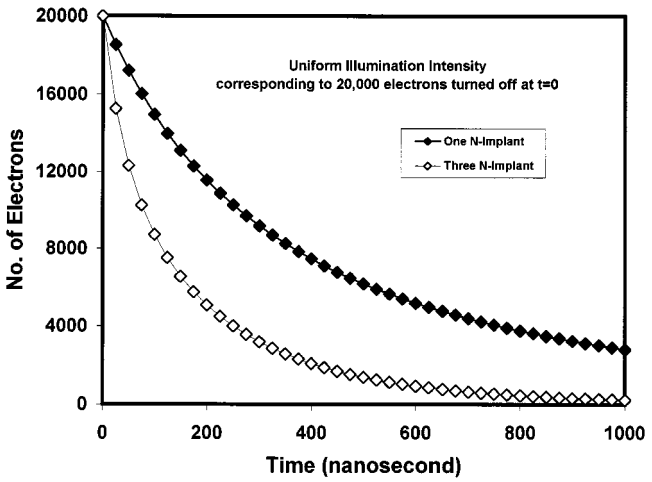

Fig. 5. Comparison between electron transfer characteristics for single n-type and three n-type implant photodetectors for uniform illumination corresponding to 20 000 electrons when the illumination is turned off at $t = 0$ showing that 90% of electrons are collected within 500 ns for the three-implant photodetector.

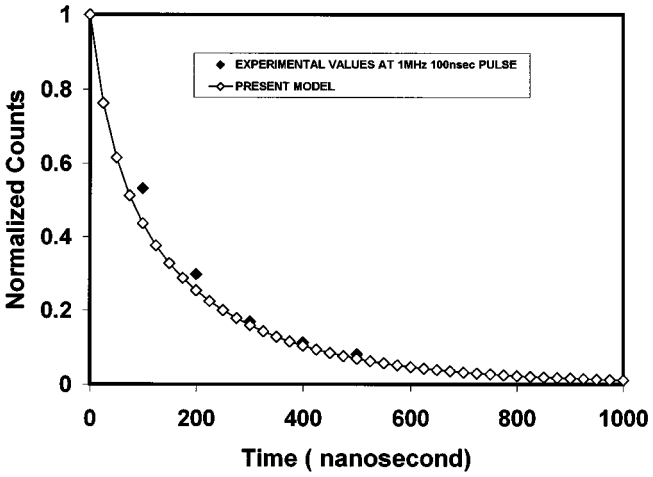

Fig. 6. Charge readout values obtained by the present model is compared with the experimental charge readout values obtained at a frame rate of 10^6 frames/s.

using the present model is shown in Fig. 6. It can be seen that the charge transfer characteristics are identical. For 90% of electron transfer the experimentally observed readout time and the readout time obtained by the present model is about 500 ns. The insignificant deviation in low time range, where only 50% of electron transfer has taken place, could be due to the simplicity of this model and the selection of number of small areas in each implanted region. If the illumination is nonuniform the scope of this model is limited as we have assumed uniform electron concentration in all the small areas and in all implanted regions.

IV. Conclusion

In conclusion, the present model takes into account the initial charge of each implant region of a multi-implant photodetector and the maximum effective transit length of the far and near electrons in addition to taking into account the fringing field effect due to graded implants. The electron transfer characteristics from each small section were obtained by considering the associated initial charge weight function under uniform illumination condition. The electron transfer characteristics, obtained for a three n-type implant photodetector was compared with that of a single n-type implant photodetector using the present model. The results obtained by this model fairly agree with the experimental values obtained by $70\ \mu\text{m} \times 45\ \mu\text{m}$ photodetector measured at a frame rate of 10^6 frames/s with uniformly illuminated by 100 ns LED pulses. This model can, therefore, be applied to five-implant or seven-implant photodetectors where the electron transit time will be further reduced.

Acknowledgment

The authors would like to acknowledge late Prof. W. F. Kosonocky for his initial idea in this subject.

References

[1] C. H. Sequin, "A charge-coupled area image sensor and frame store," *IEEE Trans. Electron Devices*, vol. ED-20, pp. 244–252, 1971.

[2] C. H. Sequin *et al.*, "Charge-coupled area image sensor using three Levels of Polysilicon," *IEEE Trans. Electron Devices*, vol. ED-21, pp. 712–720, 1974.

[3] R. H. Dyck and M. D. Jack, "Low light level performance of a charge-coupled area imaging device," in *Proc. CCD Int. Conf. Edinburgh*, 1974, pp. 154–161.

[4] R. L. Rodgers, "A 512×320 Element silicon imaging device," in *ISSCC Dig. Tech. Papers*, 1975, pp. 188–189.

[5] G. A. Antcliffe, "Development of a 400×400 element backside illuminated CCD Imager," in *CCD Conf. Proc.*, 1975, pp. 147–154.

[6] W. Steffe, "High performance 190×244 CCD area image sensor array," in *CCD Conf. Proc.*, 1976, pp. 101–108.

[7] W. F. Kosonocky and J. L. Lowrance, "High frame rate CCD imager," U. S. Patent 5 355 165, Oct. 11, 1994.

[8] W. F. Kosonocky *et al.*, "360×360-element very high frame-rate burst–image sensor," in *Proc. 1996 IEEE Int. Solid State Circuits Conf.*, San Francisco, CA, 1996, pp. 182–183.

[9] G. Yang, "Design, process, and performance simulation of a 360×360-element very high frame-rate burst–image sensor," Ph.D. dissertation, New Jersey Inst. Technol., Newark, 1996.

[10] J. E. Carnes, W. F. Kosonocky, and E. G. Ramberg, "Free charge transfer in charge coupled devices," *IEEE Trans. Electron Devices*, vol. ED-19, pp. 798–802, 1972.

[11] S. M. Sze, *Semiconductor Devices Physics and Technology*. New York: Wiley, 1985.

R. K. Jarwal was born in Indore, India, on August 16, 1962. He received the B.E. degree in electronics engineering from Devi Ahilya University, Indore, in 1985, the M.Tech. degree in nuclear engineering from the Indian Institute of Technology (IIT), Kanpur, in 1987, and the Ph.D. degree from IIT Delhi, in 1996, for his dissertation on characterization of electron cyclotron resonance discharges produced by a slotted helical antenna in mirror machine.

He is currently a Visiting Research Associate at the Department of Electrical and Computer Engineering, New Jersey Institute of Technology, Newark, NJ. His research interest is in semiconductor device fabrication and characterization, image sensors, plasma processing and rf engineering.

Durga Misra (S'84–M'88–SM'99) received the B.S. degree in physics from Utkal University in 1981, the M.Tech. in solid-state from the Indian Institute of Technology, Delhi, in 1993, and the M.S. and Ph.D. degrees, both in electrical engineering, from thr University of Waterloo, Waterloo, ON, Canada, in 1985 and 1988, respectively.

He joined the New Jersey Institute of Technology (NJIT), Newark, in September 1988, where he is now an Associate Professor in the Department of Electrical and Computer Engineering. In 1996, he served as the Director of Microelectronics Research Center, NJIT. In 1997, he was on research leave at the VLSI Research Department, Bell Laboratories, Lucent Technologies, Murray Hill, NJ. He also served as a consultant to the Sarnoff Corporation, Princeton, NJ. His general interests lie in the areas of microelectronic and optoelectronic devices and analog and digital circuit design. He has worked on CMOS and BiCMOS integrated magnetic field sensors and various other sensors. His current research interests include low power devices and circuits, and process induced damage in deep submicron CMOS devices. He has published more than 100 technical articles in international conferences and journals in circuits and devices area.

Dr. Misra received many research awards from the National Science Foundation and Industry. He has organized many international symposia on processing and devices with the Electrochemical Society. He is the Program Chair of the 2000 International Conference on Information Technology. He is a member of the Electrochemical Society and Sigma Xi.

John L. Lowrance (LS'96) received the B.S. degree in electrical engineering from the University of Tennessee, Knoxville, in 1954.

He worked for Bendix Corporation from 1954 to 1961, where he was engaged in the development of jet and rocket engine control systems. He then spent five years with the RCA Astro Division, designing television systems for TIROS, Apollo, and other space programs. In 1966, he joined the Astrophysics Department, Princeton University, Princeton, NJ, and led the development of television image sensors for space astronomy applications. He also contributed to the Stratascope II and OAO-Copernicus programs as well as several studies that culminated in the Hubble Space Telescope. In 1979, he moved to the Princeton University Plasma Physics Laboratory to develop diagnostic instrumentation for nuclear fusion research, retiring in 1989 as Head of the Diagnostic Engineering Branch. He founded Princeton Scientific Instruments, Inc. in 1980 to develop and build CCD cameras and other electro-optic systems for scientific, defense, and medical applications. He has published more than 50 papers dealing with electro-optic image sensors and systems and has been awarded six patents.

Mr. Lowrance is a member of AS and SPIE.